Ultrafast Terahertz Gating of the Polarization and Giant Nonlinear Optical Response in $BiFeO_3$ Thin Films

*Frank Chen, John Goodfellow, Shi Liu, Ilya Grinberg, Matthias C. Hoffmann, Anoop R. Damodaran, Yi Zhu, Peter Zalden, Xiaohang Zhang, Ichiro Takeuchi, Andrew M. Rappe, Lane W. Martin, Haidan Wen, and Aaron M. Lindenberg**

Ferroelectric materials comprise non-centrosymmetric unit cells with permanent electric dipole moments switchable by electric fields, exhibiting strong coupling between polarization, strain, and electronic degrees of freedom. The dynamics of the ferroelectric polarization underlies their functionality but these processes, and the speed limits determining how fast the polarization can change, remain largely unknown.[1–4] In particular, the ability to all-optically generate significant modulations or reorientations in the ferroelectric polarization represents a key step toward terahertz (THz) frequency information storage technologies, actuators, and optical modulators making use of the associated nonlinear optical response.[2–5] From a more general perspective, the use of light to modulate the functional properties of ferroelectrics holds promise for both directing these degrees of freedom and elucidating their fundamental properties.[6–8] Previous theoretical predictions indicate that large-amplitude polarization modulations can be achieved on hundreds of femtosecond timescales[9,10] and studies with hundreds of picosecond to nanosecond time resolution using electrical bias pulses have provided evidence for large amplitude modulations/switching of the polarization.[11–14] Here, we use THz pulses[15,16] as an all-optical bias to apply sub-picosecond duration electric fields to $BiFeO_3$ (BFO) thin films. We show that these generate large amplitude changes in the ferroelectric polarization and the associated nonlinear optical properties. Observed modulations in the intensity of the second harmonic light generated by the thin film correspond to on–off ratios of 220× gateable on few hundred femtosecond timescales. These effects are enhanced through the use of rare earth doping to position the sample at a morphotropic phase boundary where the electromechanical and nonlinear optical responses are magnified[17–19] but where the dynamical response of these materials has not previously been explored. Additionally, metallic electrode structures are used to both electrically bias and to further enhance the applied THz fields through subdiffraction limit focusing within a nanogap.[20–22] These results open up possibilities for wideband, high contrast THz-frequency device architectures controllable by all-optical bias fields and novel opportunities using light to dynamically modulate functional degrees of freedom in ferroelectric materials.

The second-order susceptibility of a solid, $\chi^{(2)}_{ijk}$ is responsible for nonlinear mixing and second harmonic generation (SHG) processes in solids. It is a third rank tensor whose coefficients reflect the symmetry of the medium, vanishing in centrosymmetric media under the dipole approximation.[23] For this reason, SHG is commonly used as a structural probe and in ferroelectrics, $\chi^{(2)}$ is proportional to the ferroelectric polarization.[24–28] In general, the SHG efficiency of a medium will be modified in the presence of a symmetry-breaking electric field E. An electric field induced second harmonic (EFISH) effect can be included in the frequency domain representation of the SHG process by defining a third-order susceptibility tensor $\chi^{(3)}_{ijkl}$ such that the induced nonlinear polarization at frequency 2ω in the presence of an optical field E^{ω} is given by:

F. Chen, J. Goodfellow, Dr. P. Zalden, Dr. A. M. Lindenberg
SIMES Institute for Materials and Energy Sciences
SLAC National Accelerator Laboratory
Menlo Park, CA 94025, USA
E-mail: aaronl@stanford.edu

F. Chen
Department of Electrical Engineering
Stanford University
Stanford, CA 94305, USA

J. Goodfellow, Dr. A. M. Lindenberg
Department of Materials Science and Engineering
Stanford University
Stanford, CA 94305, USA

Dr. S. Liu, Dr. I. Grinberg, Dr. A. M. Rappe
The Makineni Theoretical Laboratories
Department of Chemistry
University of Pennsylvania
Philadelphia, PA 19104, USA

Dr. M. C. Hoffmann
SLAC National Accelerator Laboratory
Menlo Park, CA 94025, USA

Dr. A. R. Damodaran, Dr. L. W. Martin
Department of Materials Science and Engineering
University of California
Berkeley, CA 94720, USA

Dr. Y. Zhu, Dr. H. Wen
Advanced Photon Source
Argonne National Laboratory
Lemont, IL 60439, USA

Dr. X. Zhang, Dr. I. Takeuchi
Department of Materials Science and Engineering
University of Maryland
College Park, MD 20742, USA

Dr. L. W. Martin
Materials Science Division
Lawrence Berkeley National Laboratory
Berkeley, CA 94720, USA

Dr. A. M. Lindenberg
PULSE Institute
SLAC National Accelerator Laboratory
Menlo Park, CA 94025, USA

DOI: 10.1002/adma.201502975

$$P_i^{2\omega} = \varepsilon_0 \sum_{j,k,l} \left[\chi_{ijk}^{(2)} + \chi_{ijkl}^{(3)} E_l \right] E_j^{\omega} E_k^{\omega *} \quad (1)$$

Because $\chi^{(2)}$ is proportional to the ferroelectric polarization, this additional $\chi^{(3)}$ term can equivalently be viewed as the first-order field-dependent Taylor-series correction term to the second-order susceptibility or ferroelectric polarization P_0. Through these approximations, our measurements probe directly the time-dependent polarization within the film with the first-order correction term a measure of the induced polarization. By scanning the polarization of the probe beam, one effectively probes the response of the medium along different crystallographic directions. The intensity measured at a detector is proportional to $[P^{2\omega}]^2$, so that the field-induced change in the second harmonic intensity, in a 1D approximation, is $\Delta I^{2\omega} \sim [I^{\omega}]^2 \left[2\chi^{(2)} \cdot \chi^{(3)} E + (\chi^{(3)} E)^2 \right]$. When an electric field is present, the intensity therefore consists of three terms: a background of order $(\chi^{(2)})^2$, a term of order $(\chi^{(3)} E)^2$ scaling quadratically with the applied field, and a cross term in which the second-order contribution acts to homodyne the EFISH signal. One can write the SHG modulation as:

$$\frac{\Delta I^{2\omega}}{I^{2\omega}} \sim 2\frac{\chi^{(3)}}{\chi^{(2)}} E + \left(\frac{\chi^{(3)}}{\chi^{(2)}} E \right)^2 \quad (2)$$

where the effective susceptibilities depend on the geometry and direction of the field vectors and may be complex valued. This demonstrates the known result that the observed modulation is a linear function of electric field strength for small applied fields. In this experiment, sub-picosecond duration THz electric fields are used to drive the SHG modulation. Related EFISH effects have been observed in a variety of material systems.[29–33]

We initially studied monodomain BFO (110) oriented ferroelectric thin films on $SrTiO_3$ substrates. Electrode structures enabled both the application of DC biases to the samples as well as the generation of field enhancements by applied single cycle THz fields (**Figure 1**).[20] Polarization-dependent static SHG measurements of these samples are consistent with the known *R3c* space group rhombohedral symmetry of BFO (Section 1, Supporting Information). Under pulsed (200 µs duration) electrical bias, we observe that the maximum modulation in the second harmonic signal occurs when the polarization of the probe beam at 800 nm is parallel to the applied DC field, indicative of a response in which the induced polarization in the sample points along the direction of the applied field. When field amplitudes larger than the known coercive fields are applied, one observes SHG butterfly loops associated with an EFISH response of BFO at low fields, followed by switching of the ferroelectric polarization (Figure 1b).[34] This can be equivalently viewed as a low-field piezoelectric response with the piezoelectric coefficient changing sign when the polarization switches.[35] The magnitude of the observed response is consistent with estimates based on known values for the piezoelectric and electrostrictive coefficients for BFO (Section 3, Supporting Information). Based on these loops, the coercive switching field is on the order of 100 kV cm^{-1}, which is consistent with reported values for this material.[36] The DC bias measurements also allow us to compare the size of the SHG modulation effects at our expected THz field strengths, which for a 400 kV cm^{-1} DC pulse corresponds to a ≈10% modulation in the second harmonic intensity.

For characterization of the ultra-fast electric-field-induced modulations, single-cycle THz pulses with peak incident electric field of 400 kV cm^{-1} generated by optical rectification in $LiNbO_3$[16,37] were applied with their electric field vector aligned in the [001] direction, parallel to the in-plane projection of the spontaneous polarization (Figure 1a). The maximum modulation in the SHG intensity was observed when both the fundamental (800 nm) and second harmonic beams (400 nm) were aligned parallel to the THz field, consistent with the results of the DC-biased EFISH measurements and again indicative of an induced polarization along the direction of the applied field vector. For small incident THz fields, the measured EFISH modulation has the same temporal dependence as the electric field as measured by electro-optic sampling (Figure 1c), consistent with the above model and indicative of a response in

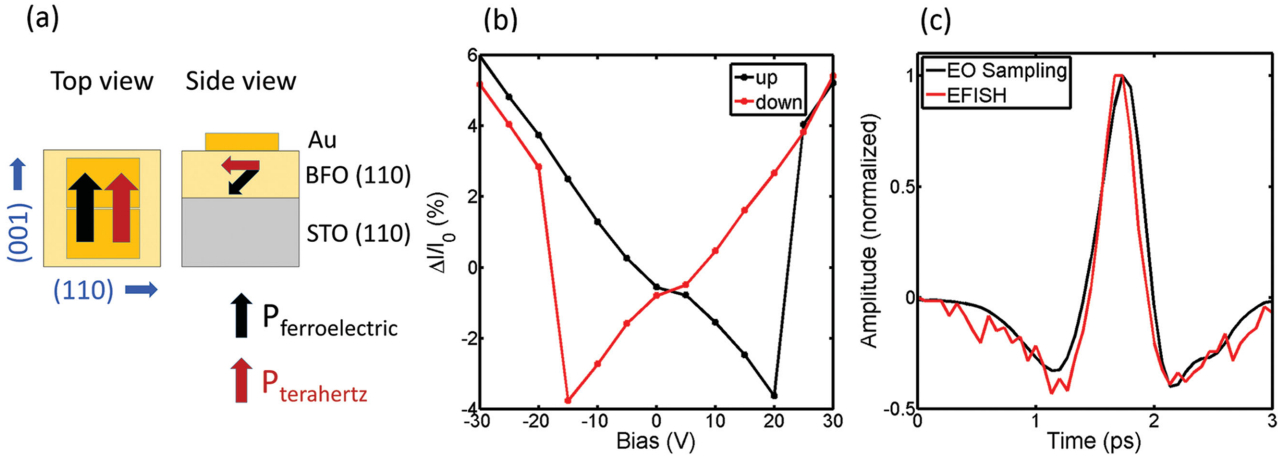

Figure 1. a) Schematic showing sample electrode structure with incident THz pump pulse. Sample orientation is shown indicating the ferroelectric and THz polarization directions. b) DC electrical biasing measurements with bias applied parallel to the ferroelectric polarization for a 2 µm gap on 60 nm BFO film showing butterfly switching loop and switching fields on the order of 100kV cm^{-1}. c) Low field THz EFISH measurement on the same BFO film shown in comparison to measured applied electric field profile measured by electro-optic sampling.

which the induced polarization follows adiabatically the applied field. This is expected for the case discussed here in which the peak of the THz spectrum (≈0.7 THz) lies significantly below the known vibrational modes of BFO.[38] In the presence of 400 kV cm^{-1} incident THz fields, we observe a modulation of the second harmonic intensity of 8%, comparable to the DC bias measurements at similar fields. Viewed from the perspective of an effective modulation in the second-order susceptibility or polarization, this corresponds to a modulation of ≈4%, roughly consistent with molecular dynamics (MD) simulations (Methods, Supporting Information). We estimate negligible (≈0.4 K) temperature jumps associated with this polarization modulation (Section 2, Supporting Information).

In order to enhance the applied THz fields and the induced modulations of the SHG efficiency and ferroelectric polarization, the same slit structure that enabled DC biasing was used, acting as a nanogap capacitor to generate field enhancements without significantly modifying the temporal shape of the applied pulse.[20,39] Section 4 in the Supporting Information describes finite difference time domain simulations modeling the field enhancement showing factors of ≈3 in the electric field within the sample. We enhance the field-driven response further by carrying out measurements on rare-earth-doped Sm–BFO (100) samples on LSAT (100) ($(LaAlO3)_{0.3}$–$(SrAl_{0.5}Ta_{0.5}O_3)_{0.7}$) substrates. A spatial gradient in the doping profile enabled measurements at a range of doping values from 0% to 45%, enabling in particular measurements near the morphotropic phase boundary between the rhombohedral ferroelectric and the orthorhombic paraelectric phase.[18,40,41] Additionally, the lower dielectric constant of LSAT enables more efficient coupling of the applied field with the thin film.[42] The expected response in the static SHG is observed as the probe beam is scanned across the doping gradient, as shown in **Figure 2**a. One observes a clear boundary in the static SHG with the intensity going to zero (red curve) at a doping concentration of ≈14% associated with the large reduction in the second-order susceptibility within the paraelectric phase, consistent with the known phase diagram[17] as well as piezoresponse force microscopy and X-ray scattering measurements of the doping-induced structural response (Section 5, Supporting Information). Figure 2a also shows the field-induced changes in the second harmonic intensity (blue curve) and on–off ratio (intensity of SHG at peak of THz field divided by intensity of SHG without THz field; green curve) as a function of doping on the bare Sm–BFO film. An enhancement is observed in both the field-induced change in the second harmonic intensity and the on–off ratio as the phase boundary is approached. This indicates that the enhancement in the on–off ratio near the phase boundary is not just associated with a reduction in $\chi^{(2)}$ but rather involves an enhancement in the effective $\chi^{(3)}$ or a variation in the relative phase of the two contributions with doping. Similar enhancements are observed in the piezoelectric response of these samples near the phase boundary.[19] Electrode structures with a width of 2 μm were deposited near this phase boundary allowing for application of enhanced ≈400 kV cm^{-1} fields within the film. At this position (corresponding to 11% Sm doping), the static SHG intensity is reduced to ≈10% of its value at zero doping, corresponding to an approximately $1/e$ reduction in the second-order susceptibility or ferroelectric polarization.

Figure 2b shows the normalized EFISH response for different applied fields measured on Sm–BFO within the electrode structure. At high fields, one observes a clear deviation in the temporal shape of the induced modulation, showing the increasing importance of the nonlinear terms, associated with a quadratic EFISH response $\approx(\chi^{(3)}E)^2$. This is additionally reflected in the frequency spectrum of the EFISH signals (Section 6, Supporting Information), which shows at the highest fields a zero-frequency component associated with rectification of the applied THz field and induced higher frequency components. One can fit well the full temporal shapes of the induced EFISH signals shown in Figure 2b, consistent with the quadratic EFISH model described above and an adiabatic response of the polarization to the applied field at the phase boundary (Section 6, Supporting Information). Figure 2c shows the field dependence of the on–off ratio within the slit. We observed a maximum on–off ratio of 220 at

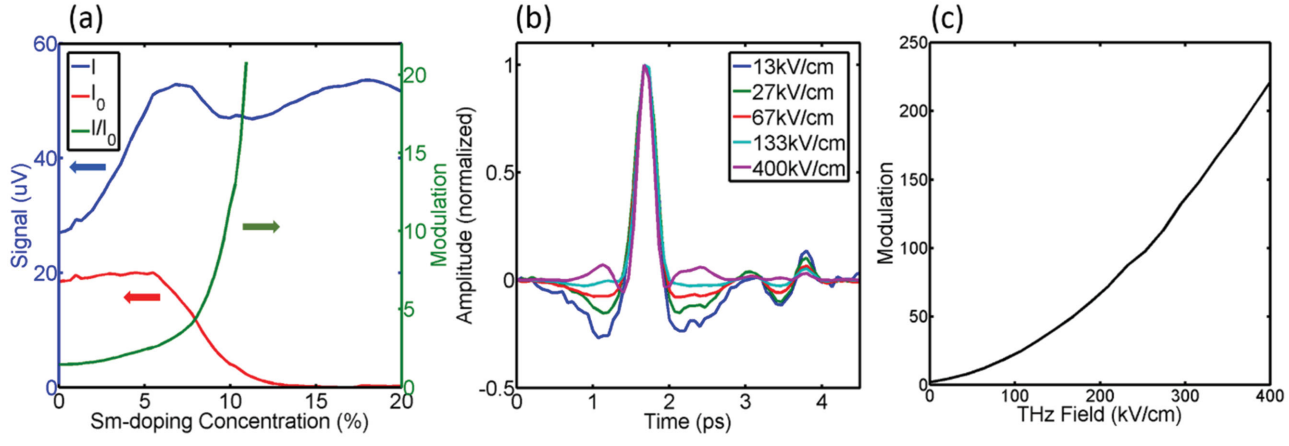

Figure 2. a) 100 nm Sm–BFO film response as a function of Sm-doping. At the morphotropic phase boundary, the sample switches from a ferroelectric to a paraelectric phase and the static second harmonic goes to zero, reflecting the centrosymmetry of the paraelectric phase (red curve). The blue curve shows the raw second harmonic intensity with THz field on. The green curve shows the on–off ratio. b) Measured normalized EFISH signal for different applied THz fields within the electrode structures near the morphotropic phase boundary (≈11% doping). c) Modulation in second harmonic intensity for Sm–BFO with electrodes as a function of peak THz field near the morphotropic phase boundary.

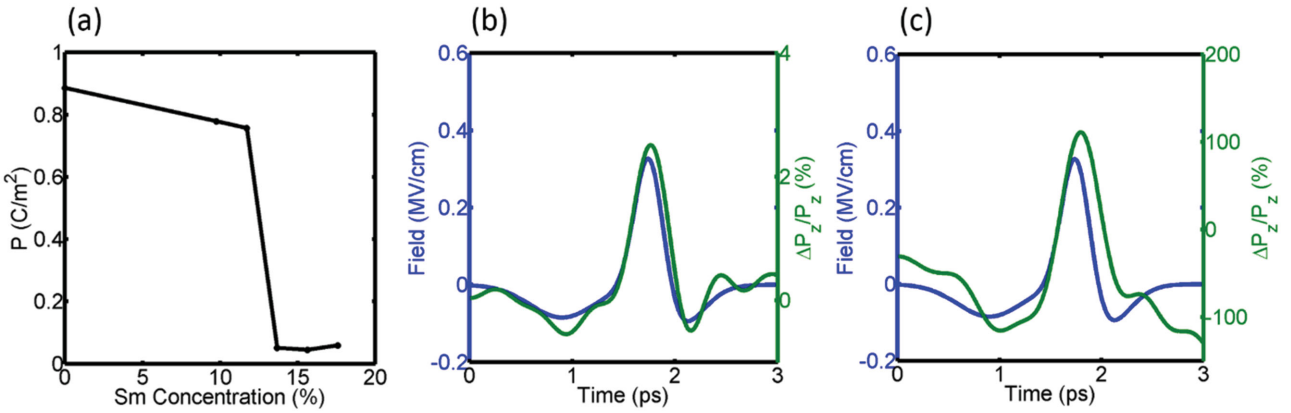

Figure 3. a) MD simulation results showing the calculated dependence of the polarization on Sm-doping. THz-driven modulation for: b) 11.7% Sm-doping and c) 13.6% Sm-doping. Note the change in polarization scale between (b) and (c).

the highest fields applied. This is ≈10× the value recorded without electrode structures and thus consistent with the estimated 3× field enhancement, and also shows that the SHG contribution from the gold electrode structures is negligible (Section 7, Supporting Information). Similar response is observed with 1400 nm probe pulses and SHG wavelength below the BFO bandgap, ruling out a resonant nonlinear optical response (Section 8, Supporting Information). MD simulations (Methods, Supporting Information) carried out for the Sm–BFO samples reproduce the known phase diagram (**Figure 3**a) and predict large-amplitude polarization modulations under THz bias, of order 100%, near the phase boundary (Figure 3b,c). These simulations additionally predict an adiabatic response of the ferroelectric polarization at the highest fields, consistent with the experiments. With $I_{2\omega} \approx |\chi^{(2)}|^2 \approx |P|^2$, $\Delta I/I \approx 2\Delta P/P + (\Delta P/P)^2$ and one directly extracts the induced fractional modulation in the polarization $\Delta P/P$ to be of order 10, a factor of about 10 higher than the MD simulations. We emphasize that the simulations do not account for the multidomain nature of the Sm–BFO film and only approximately account for the presence of the phase boundary. This estimated fractional modulation in the polarization corresponds to an experimentally induced change in polarization of ≈100 μC cm^{-2}, comparable to the built-in ferroelectric polarization away from the morphotropic phase boundary. Here one is in a non-perturbative limit where the simple approximations made above likely begin to break down and where both atomic and electronic modulations to the ferroelectric polarization likely play an important role in the field-driven response. Polarization modulations of order 10× the built-in polarization on timescales of ≈1 ps correspond to bound current densities $J \approx \Delta P/\Delta t \approx 10^9$ A cm^{-2}, comparable to estimated domain switching current densities in BFO at similar applied fields[43] and a full range of THz emission studies may be additionally applied to further elucidate this bound current response.[1]

In conclusion, we report measurements showing large amplitude modulations in the nonlinear optical response and ferroelectric polarization in multiferroic $BiFeO_3$ thin films, driven by sub-picosecond THz electric fields. These effects point toward novel applications with respect to ferroelectric photonic switches and electromechanical devices gated by all-optically applied fields. Measurements with probe energies below the band gap where the linear absorption is low show similar nonlinear responses, a key aspect with respect to device applications. Measurements of the polarization dynamics at the morphotropic phase boundary show possibilities for significantly enhancing the response of materials to ultra-fast bias fields. Straightforward extensions to nanoslit geometries with field enhancements an order of magnitude larger than used here in combination with plasmonic coupling of both THz and optical probe beams[44] point toward possibilities for manipulating the polarization and nonlinear optical properties of nanoscale ferroelectric domains on ultra-fast timescales.

Experimental Section

Epitaxial BFO films were grown by pulsed laser deposition on (110) oriented $SrTiO_3$ substrates. Monodomain BFO (110) films with P_s along [111] were obtained with thicknesses of 30 and 60 nm. Sm-doped films with thickness of 100 nm were fabricated using the combinatorial thin-film deposition technique and deposited on LSAT substrates.[45] 100 nm thick Au electrode structures were evaporated onto BFO. Slits of widths of 2 μm were defined using standard photolithography and metal liftoff techniques. SHG from the $BiFeO_3$ films was collected in reflection at normal incidence. A half-wave plate was used to control the polarization of the probe beam, and an analyzer–polarizer was used to filter the collinear second harmonic radiation. The 400 nm light was collected in a photomultiplier tube with a bandpass filter to reject the fundamental beam. See Methods in the Supporting Information for additional details on the optical setup and MD simulations.

Supporting Information

Supporting Information is available from the Wiley Online Library or from the author.

Acknowledgements

F.C. and J.G. contributed equally to this work. This work was supported by the Department of Energy, Basic Energy Sciences, Materials Sciences

and Engineering Division. Use of the Linac Coherent Light Source (LCLS), SLAC National Accelerator Laboratory, is supported by the U.S. Department of Energy, Office of Science, Office of Basic Energy Sciences under Contract No. DE-AC02-76SF00515. A.R.D. acknowledges support from the Army Research Office under Grant No. W911NF-14-1-0104. L.W.M. and H.W. acknowledge support from the Department of Energy under Grant No. DE-SC0012375. I.T. acknowledges the support from Maryland Nanocenter. Work at Argonne was supported by the U.S. Department of Energy, Office of Science, Office of Basic Energy Sciences, under Contract No. DE-AC02-06CH11357. S.L. acknowledges the support of National Science Foundation, under grant DMR-1124696. I.G. acknowledges the support of the Office of Naval Research, under grant N00014-12-1-1033. A.M.R. acknowledges the support of the Department of Energy, under grant DE-FG02-07ER46431. S.L., I.G., and A.M.R. thank the HPCMO of the DoD and the NERSC of the DoE for computational support.

Received: June 19, 2015
Revised: July 26, 2015
Published online: September 21, 2015

[1] D. S. Rana, I. Kawayama, K. Mavani, K. Takahashi, H. Murakami, M. Tonouchi, *Adv. Mater.* **2009**, *21*, 2881.
[2] T. Miyamoto, H. Yada, H. Yamakawa, H. Okamoto, *Nat. Commun.* **2013**, *4*, 2586.
[3] C. Korff Schmising, M. Bargheer, M. Kiel, N. Zhavoronkov, M. Woerner, T. Elsaesser, I. Vrejoiu, D. Hesse, M. Alexe, *Phys. Rev. Lett.* **2007**, *98*, 257601.
[4] T. Kubacka, J. A. Johnson, M. C. Hoffmann, C. Vicario, S. de Jong, P. Beaud, S. Grübel, S. W. Huang, L. Huber, L. Patthey, Y. D. Chuang, J. J. Turner, G. L. Dakovski, W. S. Lee, M. P. Minitti, W. Schlotter, R. G. Moore, C. P. Hauri, S. M. Koohpayeh, V. Scagnoli, G. Ingold, S. L. Johnson, U. Staub, *Science* **2014**, *343*, 1333.
[5] M. Mochizuki, N. Nagaosa, *Phys. Rev. Lett.* **2010**, *105*, 147202.
[6] D. Daranciang, M. Highland, H. Wen, S. Young, N. Brandt, H. Hwang, M. Vattilana, M. Nicoul, F. Quirin, J. Goodfellow, T. Qi, I. Grinberg, D. Fritz, M. Cammarata, D. Zhu, H. Lemke, D. Walko, E. Dufresne, Y. Li, J. Larsson, D. Reis, K. Sokolowski-Tinten, K. Nelson, A. M. Rappe, P. Fuoss, G. Stephenson, A. Lindenberg, *Phys. Rev. Lett.* **2012**, *108*, 087601.
[7] S. Young, A. M. Rappe, *Phys. Rev. Lett.* **2012**, *109*, 116601.
[8] B. Kundys, M. Viret, D. Colson, D. Kundys, *Nat. Mater.* **2010**, *9*, 803.
[9] S. Bhattacharjee, D. Rahmedov, D. Wang, J. Íñiguez, L. Bellaiche, *Phys. Rev. Lett.* **2014**, *112*, 147601.
[10] T. Qi, Y.-H. Shin, K.-L. Yeh, K. Nelson, A. M. Rappe, *Phys. Rev. Lett.* **2009**, *102*, 247603.
[11] P. Chen, R. J. Sichel-Tissot, J. Young Jo, R. T. Smith, S.-H. Baek, W. Saenrang, C.-B. Eom, O. Sakata, E. M. Dufresne, P. G. Evans, *Appl. Phys. Lett.* **2012**, *100*, 062906.
[12] P. Chen, M. P. Cosgriff, Q. Zhang, S. J. Callori, B. W. Adams, E. M. Dufresne, M. Dawber, P. G. Evans, *Phys. Rev. Lett.* **2013**, *110*, 047601.
[13] J. Li, B. Nagaraj, H. Liang, W. Cao, C. H. Lee, R. Ramesh, *Appl. Phys. Lett.* **2004**, *84*, 1174.
[14] A. Sharan, I. An, C. Chen, R. W. Collins, J. Lettieri, Y. Jia, D. G. Schlom, V. Gopalan, *Appl. Phys. Lett.* **2003**, *83*, 5169.
[15] T. Kampfrath, K. Tanaka, K. A. Nelson, *Nat. Photonics* **2013**, *7*, 680.
[16] K.-L. Yeh, M. C. Hoffmann, J. Hebling, K. A. Nelson, *Appl. Phys. Lett.* **2007**, *90*, 171121.
[17] D. Kan, V. Anbusathaiah, I. Takeuchi, *Adv. Mater.* **2011**, *23*, 1765.
[18] T. T. A. Lummen, Y. Gu, J. Wang, S. Lei, F. Xue, A. Kumar, A. T. Barnes, E. Barnes, S. Denev, A. Belianinov, M. Holt, A. N. Morozovska, S. V. Kalinin, L.-Q. Chen, V. Gopalan, *Nat. Commun.* **2014**, *5*, 1.
[19] D. Kan, L. Pálová, V. Anbusathaiah, C. J. Cheng, S. Fujino, V. Nagarajan, K. M. Rabe, I. Takeuchi, *Adv. Funct. Mater.* **2010**, *20*, 1108.
[20] M. Seo, H. Park, *Nat. Photonics* **2009**, *3*, 152.
[21] C. A. Werley, K. Fan, A. C. Strikwerda, S. M. Teo, X. Zhang, R. D. Averitt, K. A. Nelson, *Opt. Express* **2012**, *20*, 8551.
[22] M. Shalaby, H. Merbold, M. Peccianti, L. Razzari, G. Sharma, T. Ozaki, R. Morandotti, T. Feurer, A. Weber, L. Heyderman, B. Patterson, H. Sigg, *Appl. Phys. Lett.* **2011**, *99*, 041110.
[23] T. F. Heinz, *Second-Order Nonlinear Optical Effects at Surfaces and Interfaces*, Elsevier, Amsterdam, The Netherlands, **1991**.
[24] H. Vogt, D. Weinmann, *Phys. Status Solidi A* **1972**, *14*, 501.
[25] R. Murgan, D. R. Tilley, Y. Ishibashi, J. F. Webb, J. Osman, *J. Opt. Soc. Am. B* **2002**, *19*, 2007.
[26] E. Mishina, N. Sherstyuk, V. Stadnichuk, A. Sigov, V. Mukhorotov, Y. Golovko, A. van Etteger, T. Rasing, *Appl. Phys. Lett.* **2003**, *83*, 2402.
[27] R. C. Miller, *Phys. Rev. A* **1964**, *134*, 1313.
[28] S. A. Denev, T. T. A. Lummen, E. Barnes, A. Kumar, V. Gopalan, *J. Am. Ceram. Soc.* **2011**, *94*, 2699.
[29] C. Bao, J. C. Diels, *Opt. Lett.* **1995**, *20*, 2186.
[30] A. Mukherjee, S. Brueck, A. Y. Wu, *Opt. Commun.* **1990**, *76*, 220.
[31] W. A. Tisdale, K. J. Williams, B. A. Timp, D. J. Norris, E. S. Aydil, X. Y. Zhu, *Science* **2010**, *328*, 1543.
[32] J. I. Dadap, J. Shan, A. S. Weling, J. A. Misewich, A. Nahata, T. F. Heinz, *Opt. Lett.*, **1999**, *24*, 1059.
[33] T. A. Germer, K. W. Kołasin-acuteski, J. C. Stephenson, L. J. Richter, *Phys. Rev. B* **1997**, *55*, 10694.
[34] D. Meier, M. Maringer, T. Lottermoser, P. Becker, L. Bohatý, M. Fiebig, *Phys. Rev. Lett.* **2009**, *102*, 107202.
[35] D.-H. Do, A. Grigoriev, D. M. Kim, C.-B. Eom, P. G. Evans, E. M. Dufresne, *Integrated Ferroelectrics* **2008**, *101*, 174.
[36] D. Pantel, Y. H. Chu, L. W. Martin, R. Ramesh, D. Hesse, M. Alexe, *J. Appl. Phys.* **2010**, *107*, 084111.
[37] H. Hirori, A. Doi, F. Blanchard, K. Tanaka, *Appl. Phys. Lett.* **2011**, *98*, 091106.
[38] Z. Duan, Q. Yu, J. Wu, J. Sun, Z. Hu, J. Chu, *Thin Solid Films* **2012**, *525*, 188.
[39] M. Liu, H. Y. Hwang, H. Tao, A. C. Strikwerda, K. Fan, G. R. Keiser, A. J. Sternbach, K. G. West, S. Kittiwatanakul, J. Lu, S. A. Wolf, F. G. Omenetto, X. Zhang, K. A. Nelson, R. D. Averitt, *Nature* **2012**, *487*, 345.
[40] S. B. Emery, C. J. Cheng, D. Kan, F. J. Rueckert, S. P. Alpay, V. Nagarajan, I. Takeuchi, B. O. Wells, *Appl. Phys. Lett.* **2010**, *97*, 152902.
[41] R. J. Zeches, M. D. Rossell, J. X. Zhang, A. J. Hatt, Q. He, C.-H. Yang, A. Kumar, C. H. Wang, A. Melville, C. Adamo, G. Sheng, Y.-H. Chu, J. F. Ihlefeld, R. Erni, C. Ederer, V. Gopalan, L. Q. Chen, D. G. Schlom, N. A. Spaldin, L. W. Martin, R. Ramesh, *Science* **2009**, *326*, 977.
[42] T. Kiwa, M. Tonouchi, *Jpn. J. Apl. Phys.* **2001**, *40*, L38.
[43] A. Q. Jiang, H. J. Lee, C. S. Hwang, J. F. Scott, *Adv. Funct. Mater.* **2012**, *22*, 192.
[44] W. Cai, A. P. Vasudev, M. L. Brongersma, *Science* **2011**, *333*, 1720.
[45] M. L. Green, I. Takeuchi, J. R. Hattrick-Simpers, *J. Appl. Phys.* **2013**, *113*, 231101.